Food Research International 175 (2024) 113729

Contents lists available at ScienceDirect

Food Research International

journal homepage: www.elsevier.com/locate/foodres

Gastrointestinal delivery of codfish Skin-Derived collagen Hydrolysates: Deep eutectic solvent extraction and bioactivity analysis

Isa Silva [a,b], Bárbara M.C. Vaz [b], Sérgio Sousa [a], Maria Manuela Pintado [a], Ezequiel R. Coscueta [a,*], Sónia P.M. Ventura [b]

[a] Universidade Católica Portuguesa, CBQF - Centro de Biotecnologia e Química Fina – Laboratório Associado, Escola Superior de Biotecnologia, Rua Diogo Botelho 1327, 4169-005 Porto, Portugal

[b] CICECO – Instituto de Materiais de Aveiro, Departamento de Química, Universidade de Aveiro, 3810-193 Aveiro, Portugal

ARTICLE INFO

Keywords:
Codfish skin
Deep eutectic solvents
Marine collagen
Bioactive peptides
Colon delivery
Fishery byproducts
Nutraceutical release
Atlantic codfish
Gadus morhua

ABSTRACT

The fishing industry produces substantial by-products, such as heads, skins, bones, and scales, rich in collagen—a prevalent protein in these materials. However, further application of deep eutectic solvent-based extraction remains unexplored. In this study, we extracted collagen with urea: propanoic acid mixture (U:PA; 1:2) with a 2.2 % yield, followed by enzymatic hydrolysis with alcalase for 120 min. The resulting bioactive peptides demonstrated notable antioxidant activity (961 μmol TE) and antihypertensive properties (39.3 % ACE inhibition). Subsequently, we encapsulated 39.3 % of these hydrolysates in chitosan-TPP capsules, which released about 58 % of their content, primarily in the intestine, as mimicked in the *in vitro* model of the gastrointestinal tract. Although the digestion process did not significantly alter the size of the non-encapsulated collagen peptides, it did influence their health benefits. The promising results suggest that further research could optimize the use of collagen from fish by-products, potentially offering a sustainable source for health products.

1. Introduction

Recent trends in food processing, especially in the fishing sector, have led to increased by-products like scales, bones, skins, viscera, and heads (Bisht et al., 2021; Khawli et al., 2019). These parts are typically turned into fish oil and meal; however, research highlights their protein content for high-value product production (Khawli et al., 2019; D. P. Rodrigues et al., 2021). Atlantic codfish (*Gadus morhua*) is popular in European countries like Portugal and contains significant amounts of type-I collagen in their scales and skins (Jafari et al., 2020; Khawli et al., 2019). This collagen is a macroprotein found in tissues like tendons and skin. Its structure includes three helicoidal polypeptide α-chains, mainly characterized by the sequence $(Gly\text{-}X\text{-}Y)_n$, where X and Y often represent proline (Pro) and 4-hydroxyproline (Hyp) (Bisht et al., 2021; Coscueta, Brassesco, et al., 2021b; Jafari et al., 2020). Specifically, type-I collagen comprises about 90 % of human collagen and consists of two α1-chains and an α2-chain (C. V. Rodrigues et al., 2023).

Marine collagen is gaining interest for its biocompatibility, environmental benefits, and lack of disease or religious concerns (Espinales et al., 2023; Jafari et al., 2020). Recently, this protein has shown some promising results for food, cosmetic, and biomedical applications (Bisht et al., 2021), due to its remarkable properties including its gel-forming capacity, anti-aging effect, and its role in wound healing (Alves et al., 2017; Felician et al., 2018; Jafari et al., 2020). While acidic solvents have been the traditional method for extracting collagen, deep eutectic solvents (DES) present an eco-friendlier option, producing higher-quality collagen (Bisht et al., 2021; Coppola et al., 2020; Jafari et al., 2020). DES, formed by combining a hydrogen bond donor and acceptor, can extract collagen more effectively from codfish skins than traditional methods (Bai et al., 2017; Batista et al., 2022; Bisht et al., 2021).

In various industries like food and cosmetics, marine collagen, particularly in its hydrolyzed form, has advantages like improved solubility and gastrointestinal absorption (Ishak & Sarbon, 2018; López-Morales et al., 2019; Sun et al., 2022). Alcalase, an enzyme from the S8 endoproteinase family, is highly effective in breaking down collagen due to its selectivity, allowing shorter and more extensive hydrolysis, ideal for small peptide production (Sun et al., 2022). These peptides are valued for their health benefits, such as antioxidant properties and potential to manage health issues like collagen deficiency and cardiovascular problems (Coscueta, Brassesco, et al., 2021a; Felician et al., 2018;

* Corresponding author.
E-mail address: ecoscueta@ucp.pt (E.R. Coscueta).

https://doi.org/10.1016/j.foodres.2023.113729
Received 9 September 2023; Received in revised form 12 November 2023; Accepted 22 November 2023
Available online 29 November 2023

Himaya et al., 2012; Ishak & Sarbon, 2018). Recently, some *in vitro* and *in vivo* studies have supported these health benefits for different marine-based peptides, including a wound-healing effect in mice (Yu et al., 2023), an anti-aging effect on humans (Ito et al., 2018; Wauquier et al., 2022) and also some antioxidant and antihypertensive activities (Cho et al., 2023).

Although marine peptides have gained momentum, research on encapsulating collagen hydrolysates from Atlantic codfish skins is limited. Encapsulation methods like liposomes, metallic nanoparticles, and hydrogels propose stability and targeted peptide delivery (Felician et al., 2018; Hanachi et al., 2022; Lajmi et al., 2019; Wei et al., 2022; Yuan et al., 2018). Among these, hydrogels, particularly chitosan-based hydrogels, are gaining popularity for their adaptability, biocompatibility, and ability to enhance permeation in the gastrointestinal tract (Jafari et al., 2020; Liu et al., 2018; Ravishankar & Dhamodharan, 2020; Yuan et al., 2017, 2018). This study focuses on chitosan-TPP hydrogels, where chitosan and tripolyphosphate (TPP) interact electrostatically, resulting in gelation (Ravishankar & Dhamodharan, 2020). Using TPP with chitosan preserves peptides and reduces toxicity. These hydrogels allow controlled release, meeting the growing demand for collagen (Espinales et al., 2023). With the increasing interest in marine-based solutions, marine collagen hydrolysates offer promising prospects for blue biorefineries (Bisht et al., 2021; Prabha et al., 2020). This research aims to explore the potential of DES-extracted-collagen hydrolysates from Atlantic codfish skins, examining their encapsulation in chitosan-TPP hydrogels for targeted gastrointestinal release.

2. Methods and materials

2.1. Materials

Pascoal & Filhos S.A. (Gafanha da Nazaré, Aveiro, Portugal) provided skin of salt-cured Atlantic cod (*Gadus morhua*) that was transported to the University of Aveiro - CICECO facilities. We stored it at −20 °C after removing meat remnants, scales, and fins, and cutting it into small pieces. For skin pre-treatment, we used sodium hydroxide from Fisher Scientific (cat. no. S5881) and butyl alcohol (cat. no. A383SK-4) from VWR Chemicals. Urea (cat. no. J75826.A1) and propanoic acid (cat. no. L04210.0E) for the DES preparation came from Acros Organics (Geel, Belgium). We used NaCl from LabKem (cat. no. SOCH-00A) for collagen precipitation and a Spectra/Por® 3 dialysis membrane from Spectrum Chemical Mfg. Corp for dialysis. For SDS-PAGE analysis, we sourced the Amersham™ ECL™ Rainbow™ molecular weight marker from NZYTech (Lisbon, Portugal) and Coomassie Brilliant Blue R-250 (cat. no. #1610400) from Bio-Rad Laboratories (Hercules, California, USA). Commercial alcalase (EC 3.4.21.14; cat. no. 30079), Angiotensin-converting enzyme (ACE; EC 3.4.15.1; 5.1 $U.mg^{-1}$; cat. no. A6778), and medium-weight chitosan (deacetylation level: 75–85 %; molecular weight: 109–310 kDa; cat. no. 448877-250G) were purchased from Sigma-Aldrich (St. Louis, MO, USA). This company also supplied the non-essential amino acid solution for MEM (cat. no. M7145), sodium tripolyphosphate (cat. no. 238503), 2,4,6-Trinitrobenzenesulfonic acid solution (TNBS; cat. no. P2297), L-Leucine (ref. L-8000), pepsin (cat. no. P7000-25G), and pancreatin (cat. no. P7545). Dulbecco's Modified Eagle Medium (DMEM) high glucose (cat. no. 12-604Q) and a Penicillin-Streptomycin mix (cat. no. 17-602E) came from Lonza (Walkersville, USA), while the fetal bovine serum (FBS, cat. no. S140B) was from Biowest (Nuaillé, France). We used all other analytical grade reagents without further modification.

2.2. Marine collagen extraction

Codfish skin samples were processed following the methodology by Bisht et al. (2021), maintaining a consistent temperature of 4 °C throughout. Initially, the skins were thawed, and non-collagenous proteins removed by treating with a 0.1 M sodium hydroxide solution at a 1:10 solid–liquid ratio (SLR) for 24 h, replacing the solvent every 5–6 h. The skins were then rinsed with cold water and submerged in a 10 % butyl alcohol solution at the same SLR for 48 h, with solvent changes every 6–7 h. The biomass was then neutralized and soaked in a deep eutectic solvent (DES) urea and propionic acid solution for 48 h with continuous stirring. This DES was crafted by mixing urea and propionic acid in a 1:2 ratio, heating them until achieving a clear liquid. After cooling, the DES water content was measured and adjusted for a 0.5 M concentration. Post-extraction, the solution underwent centrifugation at 4700 g for 1 h using a Megafuge-16 centrifuge to remove insoluble particles. Collagen was then extracted using NaCl and another centrifugation step. The harvested collagen underwent dialysis against deionized water for 72 h at 4 °C, followed by storage at −80 °C before lyophilization, which enabled extraction yield calculation (Eq. (1):

$$\text{yield}(\%) = \frac{\text{weight of dried collagen (g)}}{\text{weight of dried skins (g)}} \times 100 \quad (1)$$

2.3. Collagen characterization

We characterized the extracted collagen using Fourier-transform infrared spectroscopy (FTIR), X-ray diffraction (XRD), UV–Vis spectra, and Sodium dodecyl sulfate–polyacrylamide gel electrophoresis (SDS-PAGE) (Bisht et al., 2021; Coscueta, Brassesco, et al., 2021b; Schägger & von Jagow, 1987). For the FTIR analysis, we compressed collagen samples into small disks and analyzed them using a Brucker Tensor 27 spectrometer. We obtained spectra after background subtraction, using 32 scans between 4000 and 900 cm^{-1} at 4 cm^{-1} resolution. We used dried sample disks for XRD, an Empyrean, Malvern Panalytical system, applying specific settings (Bisht et al., 2021).

We dissolved 10 mg of freeze-dried collagen in 1.5 mL of a 0.5 M acetic acid solution for UV–Vis and SDS-PAGE. We collected UV–Vis spectra between 200 and 400 nm using a Multiskan GO microplate reader (Coscueta, Brassesco, et al., 2021b). For the Tricine-SDS-PAGE, we followed a method by Schägger & von Jagow (1987). We prepared a 6 % stacking and 10 % resolving gel by mixing acrylamide, deionized water, TRIS buffer, 10 % SDS, 10 % APS and TEMED. Then, we loaded the samples and markers and ran them under specific voltage conditions. We then treated the gel with solutions to reveal protein bands (Coomassie blue R-250 (0.25 %, m/v)). Finally, we captured the resulting image using the ChemiDoc™ XRS + system and analyzed it with Image Lab™ Software, version 6.0.1.34.

2.4. Production of collagen hydrolysates

Marine collagen hydrolysates were obtained according to Sun et al. (2022) with some modifications. The lyophilized samples were initially submersed in a 75 mM phosphoric acid buffer (pH 8) in a 10 mg. mL^{-1} ratio overnight at 4 °C. Next, after a readjustment of pH to 8, the samples were placed in a boiling bath for 5 min, followed by 10 min in an ice bath. Moreover, the samples were incubated at 55 °C for 15 min, and then after adding alcalase (1:50 (m/m) enzyme-substrate ratio), the time of hydrolysis was set to start. Aliquots of 1 mL were collected at 15, 45, 120, 240, and 360 min. Each collected fraction was heated at 95 °C for 20 min to inactive the enzyme and immediately placed in an ice bath (Sun et al., 2022).

2.5. Degree of hydrolysis

To measure the degree of hydrolysis, we adapted the trinitrobenzene-sulfonic acid (TNBS) method from Hsu (2010) for a 96-well microplate. We assessed both free amine groups and those in peptide bonds using acid hydrolysis at high temperatures. Specifically, we hydrolyzed 10 mg of each freeze-dried sample in 1 mL of 6 N HCl at 110 °C for 20 h. Afterward, we neutralized the hydrolysate with 1 mL of 6 M NaOH. We used a ten-point L-Leucine standard curve, diluting a 10 mM

L-Leucine solution with 0.1 M HCl. We prepared a 0.025 % TNBS working solution daily by diluting a 5 % commercial TNBS stock. We added 50 μL of the standard or sample solution to a 96-well microplate in duplicate, along with a blank containing 50 μL of water. Then, we introduced 125 μL of a sodium phosphate buffer (pH 8.2, 75 mM) and 50 μL of the TNBS solution to each well. The sealed microplate underwent incubation for an hour at 50 °C in the dark. Using a Synergy H1 microplate reader (Biotek Instruments, Winooski, VT, USA) with Gen5 Biotek software version 3.04, we read the absorbance at 340 nm. From this, we calculated the hydrolysis degree:

$$\text{Degree of Hydrolysis}\,(\%) = \frac{h_s}{h_{tot}} \times 100 \quad (2)$$

where h_s represents the number of amino groups (as $_L$-Leucine equivalents) of each sample and h_{tot} the total number of amino groups (as $_L$-Leucine equivalents) in the original sample.

2.6. Antioxidant activity (ORAC-FL)

The oxygen radical absorbance capacity (ORAC) assay was followed according to Coscueta et al. (2019). In a broad sense, we performed a fluorescent reaction with 20 μL of each hydrolysis aliquot or standard (Trolox- concentration range: 9.98×10^{-4} – 7.99×10^{-3} μmol.mL^{-1}) mixed with 120 μL of fluorescein (70 nM) and 60 μL of AAPH (14 mM) in a black polystyrene 96 well microplate (Nunc, Denmark) in duplicate. Then, we monitored the fluorescence for 80 min with 1 min intervals at 485 nm excitation and 528 nm emission wavelengths in a Multidetection microplate reader (Synergy H1, Biotek Instruments, Winooski, VT, USA). The Trolox Equivalents (μmol TE) unit was used to express the final ORAC values (Coscueta et al., 2019, 2020).

2.7. Antihypertensive activity

The angiotensin-converting enzyme-I inhibition (iACE) assay was followed according to Coscueta et al. (2019). In a black polystyrene 96-well microplate (Nunc, Denmark) we placed 40 μL of the ACE working solution in each well, and then risen to 80 μL with ultrapure water (control) or the alcalase hydrolysate (100 μg.mL^{-1}) in triplicate. The enzymatic reaction started after adding 160 μL of a 0.45 mM substrate solution (ABz-Gly-Phe (NO_2)-Pro), with incubation at 37 °C. Then, we monitored the fluorescence for 30 min at 350 nm excitation and 420 nm emission wavelengths in a Multidetection microplate reader (Synergy H1, Biotek Instruments, Winooski, VT, USA). The percentage of ACE activity inhibited was used to express the antihypertensive activity (Coscueta et al., 2019).

2.8. Peptide size profile

High-Performance Size Exclusion Chromatography (HPSEC) was performed precisely following the methodology described by Fernandez Cunha et al., (2023). The injection volume of each sample was 10 μL, and all samples were previously run through PTFE/L 0.22 μm filters.

2.9. Encapsulation of collagen hydrolysates in Chitosan-TPP capsules

We encapsulated collagen hydrolysates in chitosan-TPP capsules, adapting the method from Yuan et al., (2018) with modifications (Yuan et al., 2017). We first mixed a 3 % chitosan solution using 3 % acetic acid and stirred it for 1 h. Each collagen hydrolysate's pH was adjusted to 4 using a 1 M HCl solution, then combined with the chitosan solution in a 1:3 ratio. After stirring this mix at 900 rpm for 30 min, it rested for 20 min to release trapped air bubbles.

We prepared a 0.4 % TPP gelling solution using sodium TPP and ultra-pure water. For capsule preparation, 1 g of our gel-forming solution went into a 3 mL plastic syringe with a 10 μL micropipette tip. We added 2 mL of the TPP solution to a beaker. Using a Programmable Double Syringe Pump (World Precision Instruments; Sarasota, USA), we extruded the solution dropwise into the TPP solution from a height of approximately 9/10 cm at a 50 μL min^{-1} flow rate and 900 rpm. Following extrusion, we let the capsules settle for 20 min, then rinsed them twice with distilled water. We lyophilized the cleaned capsules and stored them at room temperature (Zeng et al., 2021).

For encapsulation efficiency, we analyzed samples via HPSEC. Following the encapsulation ratios, we diluted the original hydrolysate sample and tested the residual TPP solution from capsule production (Yuan et al., 2017). We calculated the encapsulation percentage using (Eq. (3):

$$\text{Encapsulation efficiency}\,(\%) = \frac{(A_h \times V_t) - (A_{rgs} \times (V_t - V_{bw}))}{(A_h \times V_t)} \times 100 \quad (3)$$

where A_h is the area of the resulting HPSEC chromatogram of the diluted hydrolysate; V_t corresponds to the total volume after the capsule formation step (3 mL); A_{rgs} is the area of the resulting HPSEC chromatogram of the remaining gelling solution (TPP), and V_{bw} corresponds to the volume of water content in the capsules (moisture).

2.10. Reverse phase HPLC: Collagen hydrolysate polarity

Reverse Phase High-Performance Liquid Chromatography (RP-HPLC) was performed using a reverse phase column (AdvanceBio Peptide Map column 2.1 × 150 mm, 2.7-μm). Peptide separation was performed with a mobile phase A – water-0.1 % TFA – and a mobile phase B – acetonitrile-0.1 % TFA. The operating conditions were isocratic elution for 3 min at 100 % phase A, followed by a gradient until reaching 16 % phase B at 30 min, 45 % phase B at 46 min, 95 % phase B at 47 min, isocratic elution for the next 2 min, and return to 100 % phase A at 50 min, all at a continuous flow of 0.3 mL.min^{-1}. Chromatographic analysis was carried out using a Waters e2695 separation module system connected to a UV/Vis photodiode array detector (PDA, 190–600 nm). The injection volume of each sample was 20 μL, and all samples were previously filtered using PTFE/L 0.22 μm filters.

2.11. Scanning electron microscopy (SEM)

Dried chitosan-TPP capsules morphology was examined with a Phenom XL G2 (Thermo Fischer Scientific, The Netherlands) scanning electron microscope (SEM). A control capsule without any peptide content was also prepared and analyzed. These capsules were thoroughly cut in half using a scalpel and placed on top of the observation pins, which were covered with double-sided adhesive carbon tape (NEM tape; Nisshin, Japan). Afterward, the samples were coated with gold/palladium on a sputter coater (Polaron, Germany) and visualized. SEM analyses were performed with the equipment operated at a high-vacuum (1.0 Pa) and an accelerating voltage of 5 kV, using the secondary electron detector (SED).

2.12. FTIR analysis

Regarding the FTIR analysis, chitosan-TPP with U:PA hydrolysate (UPAH), and the control capsule were analyzed. Furthermore, these samples were submitted into a Fourier Transform Infrared Spectrometer (FTIR) (PerkinElmer Spectrum-100), with a horizontal attenuated total reflectance accessory, and a diamond/ ZnSe crystal. All spectra were acquired in duplicates with 32 scans, 4 cm^{-1} resolution, and collected between 4000 and 600 cm^{-1} (Coscueta, Sousa, Reis, & Pintado, 2021).

2.13. Gastrointestinal tract simulation

The INFOGEST protocol proposed by Brodkorb et al. (2019) was adapted for gastrointestinal simulation. Two different assessments were

realized in parallel: one simulation to study the release of collagen hydrolysates from chitosan-TPP capsules in the conditions of the gastrointestinal tract (Test A) and another one to detect variation of non-encapsulated peptide size during digestion, as well as its structural changes to enzyme action (Test B). Both assays were divided into 3 stages: i) oral phase using a simulated salivary fluid (SSF) at pH 7 for 2 min; ii) gastric phase with a simulated gastric fluid (SGF) at pH 3 for 120 min; iii) intestinal phase using a simulated intestinal fluid (SIF) at pH 7 also for another 120 min. Before the simulation of the gastrointestinal digestion, all simulated fluids were pre-warmed at 37 °C, and all samples were neutralized to pH 7.

2.13.1. Test A: Controlled peptide release

For test A, 20 mg of chitosan-TPP capsules with incorporated collagen hydrolysate were weighted and submitted to the INFOGEST protocol. However, since chitosan cannot be broken down by the digestive enzymes in the human stomach and small intestine, the impact of digestive enzymes was not considered (Yuan et al., 2017). The simulation was initiated by adding the oral phase components and mixing them for 2 min using a vortex. After that, the samples were set to pH 3 with HCl 1 M. After adding SGF and placing it in the orbital shaker at 37 °C and 130 rpm, the gastric phase was started. After 2 h, the intestinal phase began by adjusting pH to 7 with NaOH 1 M, adding SIF, and reducing the shaking to 45 rpm. Five aliquots were collected throughout the simulation: one in the oral phase and two in the gastric and intestinal phases (after 1 and 2 h, respectively). A heat shock treatment was done to stop the reaction, setting the aliquots at 80 °C for 15 min (Brodkorb et al., 2019). The obtained fractions were also submitted to HPSEC, ORAC-FL, and iACE assays (Coscueta, Brassesco, et al., 2021a; Coscueta et al., 2019; Yuan et al., 2017).

2.13.2. Test B: Gastrointestinal peptide digestion

For test B, 1 mL of each hydrolysate or control (with distilled water) was placed in the corresponding recipients and submitted to INFOGEST protocol (Brodkorb et al., 2019). In contrast to Test A, this simulation includes digestive enzymes, except for amylase and lipase, since the samples are not substrates for these enzymes. Digestion was initiated by adding the oral phase components and mixing them for 2 min with a vortex. After that, all samples were set to pH 3 by adding HCl 1 M. The gastric phase was started using an orbital shaker at 37 °C and 130 rpm after adding SGF, water, $CaCl_2$, and the pepsin solution. After 2 h, the intestinal phase began once readjusting pH to 7 with NaOH 1 M and adding SIF, water, $CaCl_2$, and the pancreatin solution. The shaking was reduced to 45 rpm. In this gastrointestinal simulation, one aliquot (500 μL) of each digestion stage was collected for HPSEC, ORAC-FL, and iACE assays (Coscueta, Brassesco, et al., 2021a; Coscueta et al., 2019; Yuan et al., 2017). A heat shock treatment was done to stop the reaction by setting the aliquots at 80 °C for 15 min (Brodkorb et al., 2019).

2.14. Biocompatibility

After simulating the digestion, the hydrolysates were tested *in vitro* for metabolic inhibition on Caucasian colon adenocarcinoma (Caco-2, ECACC86010202) cells. These cells were maintained in DMEM (Dulbecco's Modified Eagle Medium) high glucose supplemented with 10 % (v/v) of FBS, 1 % (v/v) penicillin–streptomycin, and MEM (Minimum Essential Medium) non-essential amino acid solution. Then, the culture was incubated at 37 °C in a humidified condition with 5 % (v/v) of CO_2. TrypLE Express (Thermo Scientific, Waltham, MA, USA) was used to separate the cells, which were then seeded (1×10^5 cells *per* well) into 96-well Nunc Optical Btm Plt PolymerBase Black microplates and incubated for 24 h. After sterile filtering, the culture media was carefully removed and replaced with sample aliquots. After a 24 h incubation period, the metabolic inhibition was assessed by Presto Blue™ HS Cell Viability assay (ThermoScientific, Waltham, MA, USA), following the manufacturer's instructions. The fluorescence was read using a multi-detection microplate reader (Synergy H1, Biotek Instruments, Winooski, VT, USA) with excitation and emission wavelengths of 560 nm and 590 nm, respectively. Wells without cells were considered as blanks, while cells in culture media served as the control. The metabolic inhibition was calculated according to (Eq. (4):

$$\%\ \text{metabolic inhibition} = \frac{(F_{control} - F_{sample})}{F_{control}} \times 100 \quad (4)$$

where $F_{control}$ and F_{sample} are the fluorescence intensities at 590 nm of control and sample, respectively (Coscueta, Sousa, Reis, & Pintado, 2021).

2.15. Statistical analysis

The results of the enzymatic hydrolysis and gastrointestinal simulations (Test A and B) were statistically evaluated by a one-way analysis of variance (ANOVA) followed by Tukey's post hoc test. The general difference between the mean values of the Degree of Hydrolysis, antioxidant, and antihypertensive activities in marine collagen extracted with U:PA mixture was considered. Separation of means was conducted by the least significant difference at a 5 % probability level. The statistical analysis was carried out using Origin 9.0.0 software in the 64-bit version.

3. Results and discussion

3.1. Marine collagen extraction and characterization

Based on the extraction methodology by Bisht et al. (2021), we chose a urea and propanoic acid (1:2) mixture to extract marine collagen. We achieved a collagen yield of 2.2 ± 0.3 %. This is lower than the 5.0 % yield reported for marine collagen extracted with U:PA (UPAC) (Bisht et al., 2021), possibly due to variations in fish species, sex, maturity, seasonal changes, and catchment region. The relationship between these factors and collagen content remains under-explored (Jafarpour et al., 2020). Factors like temperature, time, and solvent concentration also impact marine collagen extraction, necessitating parameter optimization for best results (Jafari et al., 2020).

Fig. 1 offers a comprehensive marine collagen characterization featuring results from SDS-PAGE, UV–Vis, FTIR, and X-ray diffraction analyses. In the SDS-PAGE gel (Fig. 1A), we identified four primary bands matching collagen's standard subunits (α1 and α2) and others (β and γ) indicating collagen crosslinking both within and between molecules (Coscueta, Brassesco, et al., 2021b). Some faint bands under 110 kDa suggest potential contamination from non-collagenous proteins or type-I collagen degradation (Bisht et al., 2021). These bands might also arise from glycoproteins associated with collagen, impacting purity and yield (Felician et al., 2018).

The UPAC UV–Vis spectrum (Fig. 1B) demonstrates an intense peak near 231 nm and a milder one around 280 nm, comparable to commercial collagen. These peaks verify the presence of our target protein. Existing literature suggests that peak intensity in the 210–240 nm range signifies collagen's triple helical structure, potentially due to transitions in the peptide bond or specific groups in polypeptide chains. These findings, coupled with the noted absorbance at 280 nm from aromatic amino acids, affirm the existence of non-collagen proteins, consistent with our SDS-PAGE analysis (Coscueta, Brassesco, et al., 2021b).

Diving deeper, the UPAC FTIR spectrum (Fig. 1C) showcases five dominant vibration modes (Amide A, B, I, II, and III) mirroring commercial collagen (Bisht et al., 2021; Carvalho et al., 2018). These vibrations reveal valuable information about the collagen's molecular components and structure. Amide A corresponds to infrared absorption of N-H stretching, typically between 3400 and 3440 cm^{-1} (Carvalho et al., 2018). In our sample, this vibration appears at 3286 cm^{-1}, probably due to a hydrogen bond of an NH group leading to a shift to

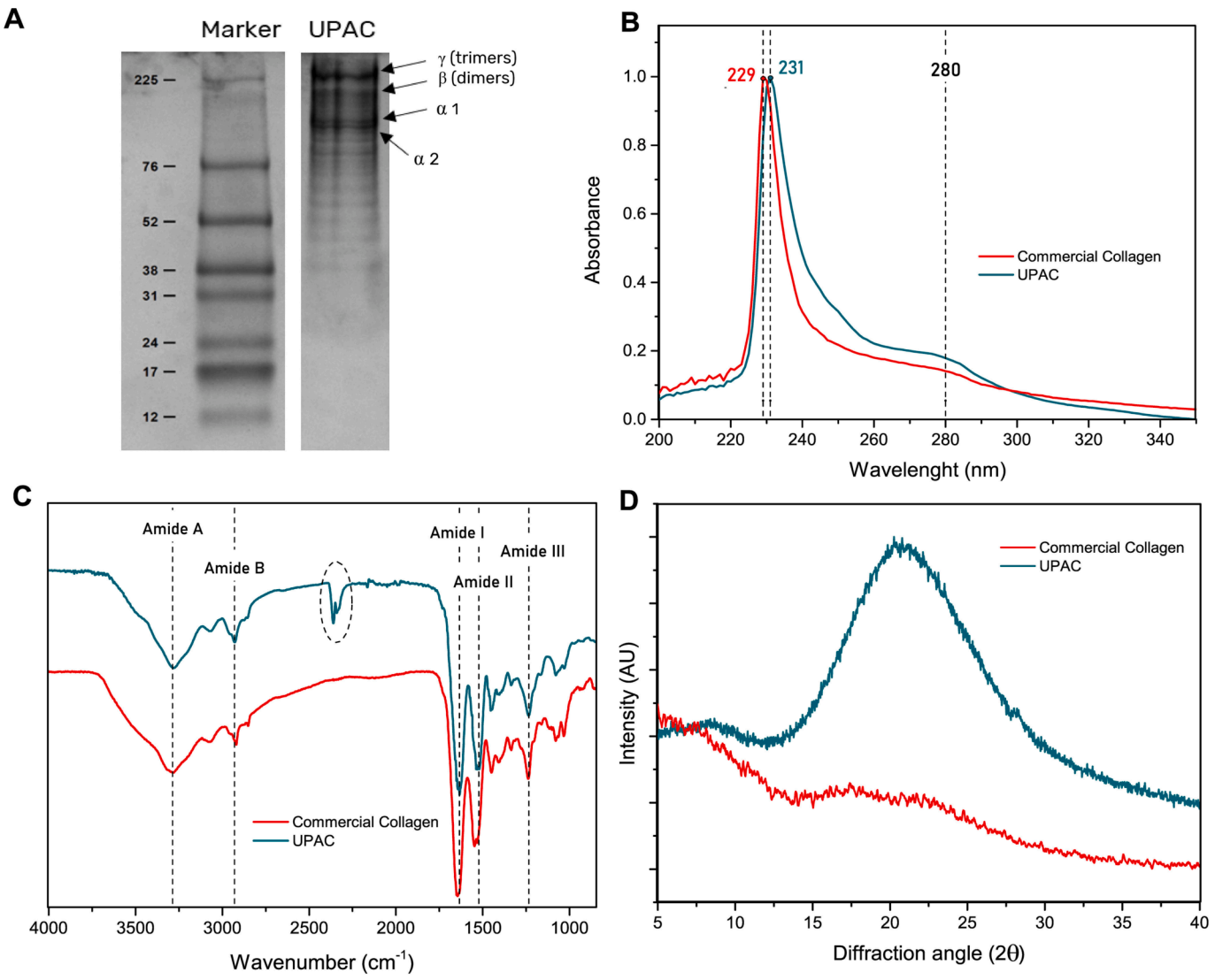

Fig. 1. Characterization results of marine collagen extracted with U:PA (UPAC); A) SDS-PAGE electrophoretic patterns; B) UV–Vis resulting spectra; C) FTIR resulting spectra; D) X-Ray Diffraction resulting spectra.

lower frequencies (Bisht et al., 2021). Moreover, amide B corresponds to CH_2 asymmetrical stretch absorbed at 2929 cm^{-1} (Bisht et al., 2021; Carvalho et al., 2018). Amide I is a characteristic C = O stretching vibration peak commonly found in the 1600 to 1700 cm^{-1} range. In the control and UPAC samples, this amide is at 1634 cm^{-1}. Amide II, corresponding to N-H bending vibrations, is absorbed in 1538 cm^{-1}. Finally, amide III indicates the presence of a triple helix structure by identifying C-N stretching and N-H in-plane bending from amide linkages and absorptions from CH_2 groups of glycine backbone and proline side chains (Carvalho et al., 2018). In UPAC, amide III appears at 1236 cm^{-1}. Intriguingly, the UPAC sample exhibits a distinct peak between 2500 and 2250 cm^{-1}, likely due to CO_2 signals resulting from imprecise background subtraction. A crucial indicator of high-quality triple helical structures is a close approximation to 1 for the ratio of amide III to 1450 cm^{-1} (Bisht et al., 2021; Carvalho et al., 2018). Our extracted collagen's ratio was 0.9656, indicating that most of it retains its native form.

In the X-ray diffraction spectrum (Fig. 1D), UPAC reveals two primary peaks, aligning well with the general attributes of collagen reported in the literature (Bisht et al., 2021; Oliveira et al., 2021). By comparison, commercial collagen displays slightly varied intensity values.

Overall, our U:PA (1:2) mixture successfully extracts type-I collagen from Atlantic codfish skins. Still, our findings also spotlight pure and slightly impure collagen forms, including the triple helix structure and its denatured variants. These results, combined with evidence of non-collagenous proteins, emphasize the need for refining the extraction procedure, especially for large-scale operations. We also see merit in exploring the influence of biomass differences further. While our study's primary aim was not extraction optimization—currently a work in progress—the obtained samples aptly serve our exploration of collagen hydrolysates for potential health benefits.

3.2. *Enzymatic hydrolysis*

To produce the best UPAC hydrolysate (UPAH), we performed enzymatic hydrolysis using alcalase for 6 h, recovering many aliquots at different times (15, 45, 120, 180, 240, and 360 min) and subsequently evaluated their degree of hydrolysis (Fig. 2A), antioxidant (Fig. 2B) and antihypertensive (Fig. 2C) activities, plus their peptide profile (HPSEC) (Fig. 3).

3.2.1. *Degree of hydrolysis*

Fig. 2A reveals hydrolysis values rose from 28.7 % at 15 min to 56.5 % at 120 min, demonstrating alcalase's efficacy in breaking down

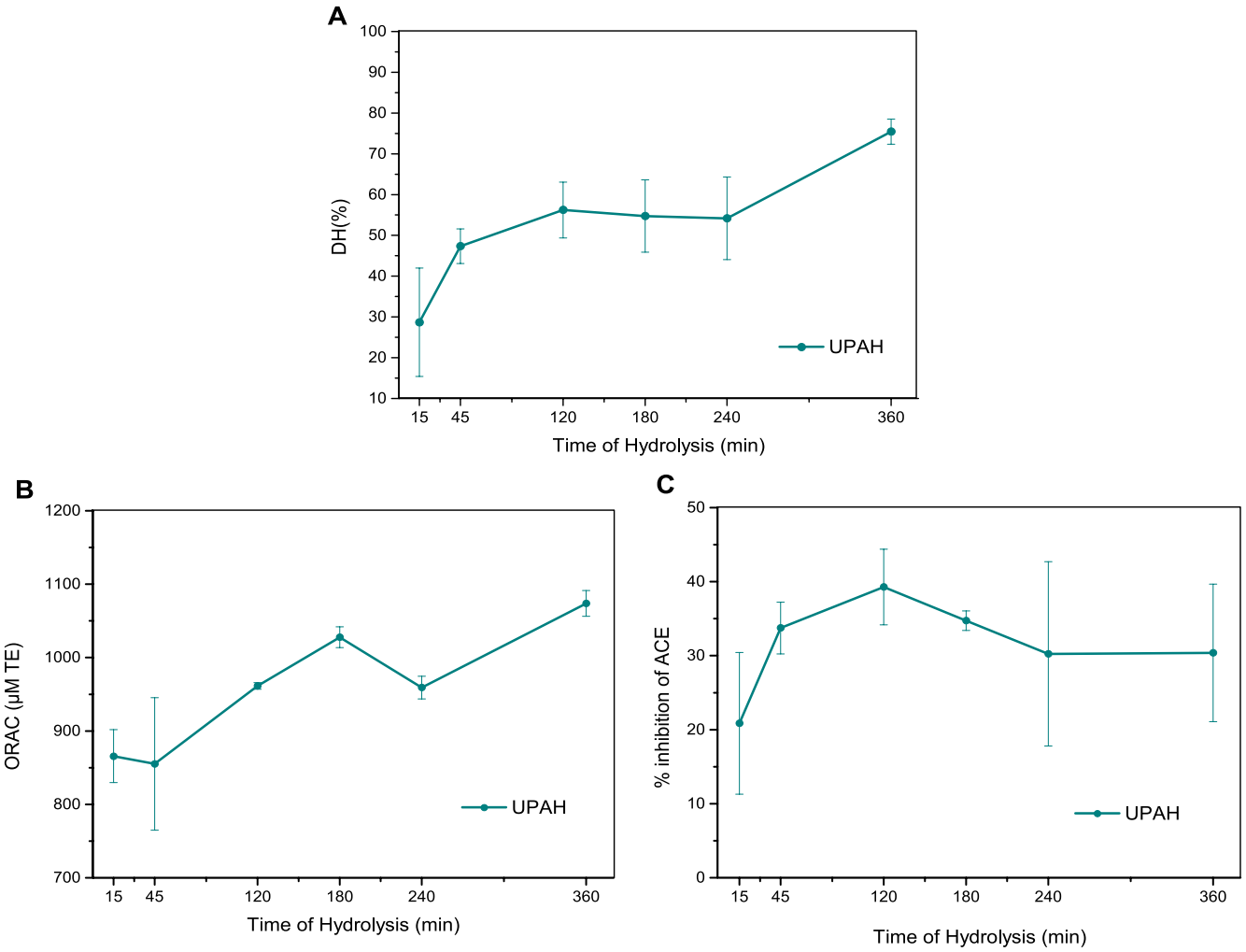

Fig. 2. Variation of hydrolysis parameters of UPAH over time (min); **A**) Degree of hydrolysis (DH); **B**) Potential antioxidant activity (ORAC; μM in Trolox Equivalents); **C**) Potential antihypertensive activity (iACE in the percentage of inhibited ACE).

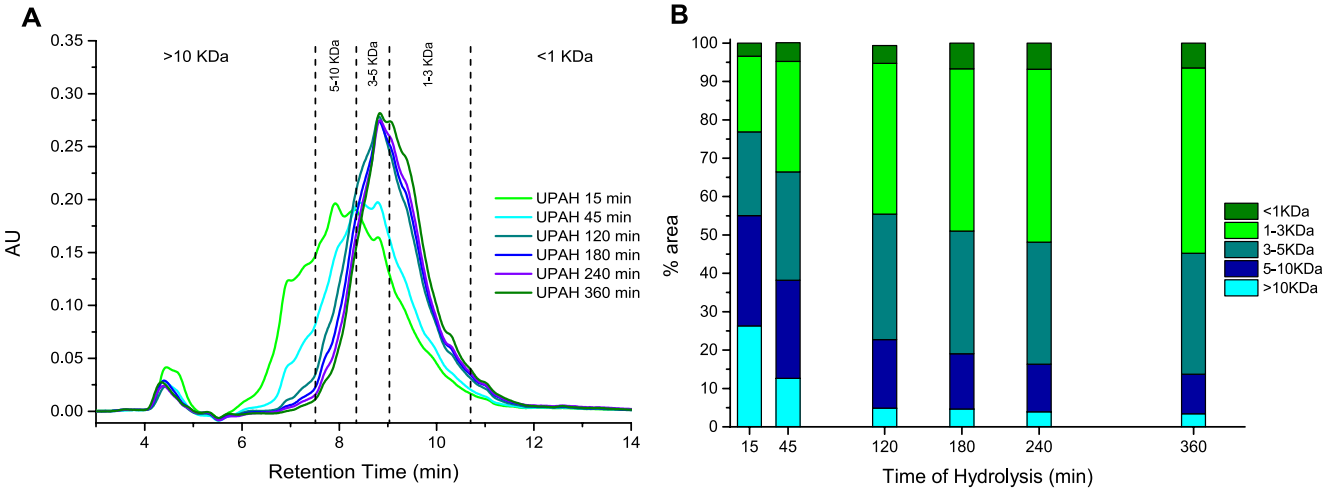

Fig. 3. Peptide size distribution analysis. **A**) UPAH HPSEC chromatogram of absorbance versus retention time in different hydrolysis times; **B**) Molecular weight distribution of UPAH peptide size based on HPSEC areas.

collagen. This enzyme's selectivity towards amino acids such as Glu, Met, Leu, Tyr, and Lys might explain the observed variations in hydrolysis (Sun et al., 2022). A more detailed look into the amino acid composition of UPAH could provide further insights. While earlier research noted hydrolysis levels for acid-based marine collagen peptides, findings for DES-based peptides remain scarce. For instance, Sun et al. (2022) found hydrolysis rates ranging from 9.07 % to 15.73 % in tilapia skin bioactive peptides over varying durations. Similarly,

Vázquez et al. (2019) reported rates between 85.2 % and 90.6 % in various fish species after a 4 h hydrolysis period using a different method.

3.2.2. Antioxidant and antihypertensive activities

Fig. 2B's ORAC analysis reveals an antioxidant value of 866 μM TE at 15 min, climbing to 961 μM TE at 120 min, and reaching 1074 μM TE at 360 min. While marine collagen peptides are known for antioxidant activity, their exact action remains unclear (Felician et al., 2018). This activity can be influenced by factors like aromatic amino acid content and lower molecular weights (Mw). Collagen's Gly and Pro are advantageous in scavenging ROS (Chi et al., 2014; Coscueta, Brassesco, et al., 2021a; Felician et al., 2018). Antioxidant properties have been found in collagen hydrolysates from various marine sources, like Spanish mackerel (*Scomberomorus maculatus*) skin (Chi et al., 2014), salmon (*Salmo salar*) by-products(Neves et al., 2017; Wu et al., 2018), dark tuna (*Thunnus orientalis*) muscle by-product (Hsu, 2010), sea cucumber (*Parastichopus tremulus*) (Mildenberger et al., 2021), goby fish (*Pomatoschistus microps*) (Nasri et al., 2021), and even already from Pacific cod (*Gadus macrocephalus*) (Himaya et al., 2012) and Atlantic cod (*Gadus morhua*) (Coscueta, Brassesco, et al., 2021a) skins.

The UPAH shows a maximum of 39.3 % ACE inhibition at 120 min (Fig. 2C). While the exact relationship between structure and ACE-inhibitory peptide activity remains undefined, research points to the C-terminal tripeptide sequence of collagen peptides as a critical player in ACE binding. Collagen's Hyp-Gly-Pro tripeptide sequence is an effective ACE inhibitor (Felician et al., 2018; Sun et al., 2022). Prolonged exposure to the alcalase can lead to over-hydrolysis, where peptides are broken down into smaller fragments or amino acids that may not possess the same antihypertensive properties (Agyei et al., 2016). Optimal peptide size is crucial for specific bioactivities, and excessively small peptides might lose their functional conformation and effectiveness. Also, prolonged hydrolysis can trigger secondary reactions, such as the formation of peptide aggregates or the interaction of peptides with other components in the reaction mixture (Zhang et al., 2017), potentially reducing their bioavailability and antihypertensive activity. Moreover, over time, the bioactive peptides might undergo structural changes due to environmental factors (like pH and temperature) or reactions with other molecules, decreasing their biological activity (Gharibzahedi et al., 2022). So, prolonged hydrolysis can notably impact this sequence, reducing antihypertensive activity, as evidenced in Fig. 2C after the 120-min hydrolysis period.

Recent research has identified ACE-inhibitory peptides in marine by-products, using substrates like HHL (Hippuryl-Histidyl-leucine) (Ahn et al., 2012; Himaya et al., 2012; Sun et al., 2022), FAPGG (Furanacryloyl-prolyl-glycyl-glycine) (Vázquez et al., 2019), and Abz–-Gly–Phe(NO_2)–Pro (Coscueta, Brassesco, et al., 2021a). ACE-inhibitory effects have also been observed in salmon waste (Ahn et al., 2012), and Pacific (Himaya et al., 2012) and Atlantic cod skin (Coscueta, Brassesco, et al., 2021a), among others (Vázquez et al., 2019).

3.3. Peptide size

We collected different fractions during hydrolysis. Using HPSEC, we analyzed peptides in the hydrolysates based on molecular size. Larger peptides came out first, while smaller ones followed. Fig. 3A displays this size distribution profile.

At the 15 min fraction, we observed two peak distributions: one around 4 min and another near 8 min. Over time, the UPAH became richer in smaller peptides, shifting the chromatogram to the right. We categorized these peptides into five weight ranges: >10 kDa, 5–10 kDa, 3–5 kDa, 1–3 kDa, and < 1 kDa. Fig. 3B shows the percentage distribution of these ranges over time. At 15 min, 29 % of peptides were in the 5–10 kDa range. From 45 to 360 min, the 1–3 kDa range dominated, making up an increasing portion of the total, from 29 % to 48 %. Peptide size and sequence play crucial roles in their bioactivities (Chi et al., 2014; Himaya et al., 2012). Smaller peptides, especially those in the 1–3.5 kDa range or below 1 kDa, showcase potent (Himaya et al., 2012; Ishak & Sarbon, 2018). Peptides of lower weights tend to have robust antioxidant properties and can stabilize free radicals. Additionally, these smaller peptides stand a good chance of crossing the intestinal barrier and retaining their activity post-absorption (Chi et al., 2014).

Considering these findings, we chose a 120-min hydrolysis duration, that we also used for the next steps. By this point, we noticed significant changes in peptide content, antioxidant value, and hydrolysis degree. A shorter hydrolysis time also promotes process viability, requiring less energy and resources.

3.4. Encapsulation of collagen hydrolysates in chitosan-TPP capsules

Using the extrusion method, we created two chitosan-TPP capsules: a control without peptides and one with UPAH encapsulated. By comparing HPSEC chromatogram areas of hydrolysates and the rinse effluent, we found that the chitosan-TPP matrix entrapped 39.3 % of the peptide content. However, on the lower side, this efficiency could result from a less robust structure due to reduced chitosan-TPP interactions or specific peptide characteristics. Peptides with lower molecular weight, lacking a clear secondary structure, might readily diffuse through the capsules. The polarity of the peptide might also impact its entrapment (Yuan et al., 2018).

Several factors influence the structure and ionic interactions of chitosan-TPP, including chitosan's molecular weight and concentration, TPP concentration, pH, and ionic strength (Du et al., 2019; Nasri et al., 2021; Yuan et al., 2017). Chitosan's molecular weight impacts chain extension, polydispersity, and capsule size. Du et al. (2019) stated that adequate chitosan Mw is near 100 kDa since it facilitates the interaction with encapsulated peptides. We used chitosan in the Mw range of 190–310 kDa, which might decrease chitosan-hydrolysate interactions and alter the capsule size. Chitosan concentration and pH play a role in determining available $-NH_3^+$ groups crucial for ionic interactions with TPP, encapsulated peptides, and adhesion to mucin glycosyl in gastrointestinal delivery (Du et al., 2019; Nasri et al., 2021). Increasing the concentration of the encapsulated samples produces a more compact capsule structure with a smaller mesh size, reducing earlier peptide leach (Yuan et al., 2017). Recent studies have shown that TPP concentration is crucial to this encapsulation type. Until recently, literature has reported contradictory results regarding the entrapment efficiency by varying the TPP concentration. Yuan et al. (2017) produced chitosan-TPP capsules in the range of 0.1 to 10 % of TPP (m/m) and concluded that smaller concentrations (~0.4 %) had improved the entrapment efficiency of BSA. It is essential to note that using complex proteins for encapsulation differs from collagen peptides, underscoring the need for additional research.

We assessed peptide polarity with Reverse Phase-HPLC (RP-HPLC). Fig. 4A depicts the UPAH chromatogram and the capsule production rinse solutions. Most hydrolysate collagen peptides are hydrophilic, evident from the notable early peak. The rinse solutions reveal that many polar peptides were not encapsulated, suggesting potential changes to the hydrolysate's bioactive potential (Fig. 4B).

3.5. Capsule morphology

The resulting dried capsules were morphologically spheric and uniform, approximately 3.33 ± 0.46 mm in diameter. Moreover, using 1 g of gelling solution at 50 μL min^{-1} pumping flow rate produced approximately 30 to 40 capsules. The size and number of capsules can be related to the peptide content. Adding more peptides increases the average capsule diameter (Nasri et al., 2021). We used SEM to observe the surface and interior of both control and chitosan-TPP + UPAH capsules (Fig. 5).

The spherical shape and smooth surface account for the established ionic interactions between chitosan and TPP. When comparing the

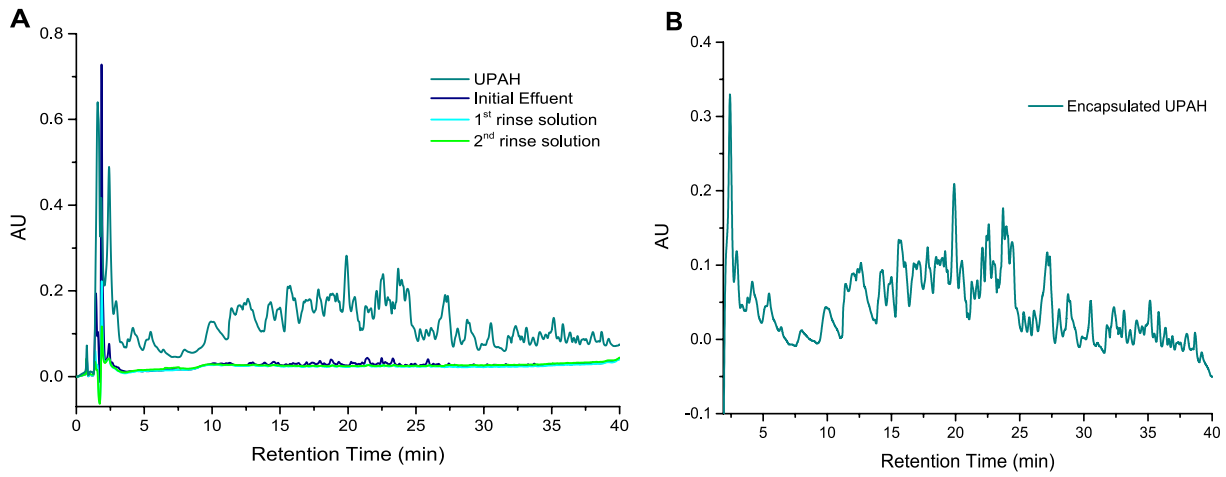

Fig. 4. Reverse Phase-HPLC chromatogram; **A**) UPAH and rinse solutions of chitosan-TPP + UPAH production; **B**) Encapsulated UPAH.

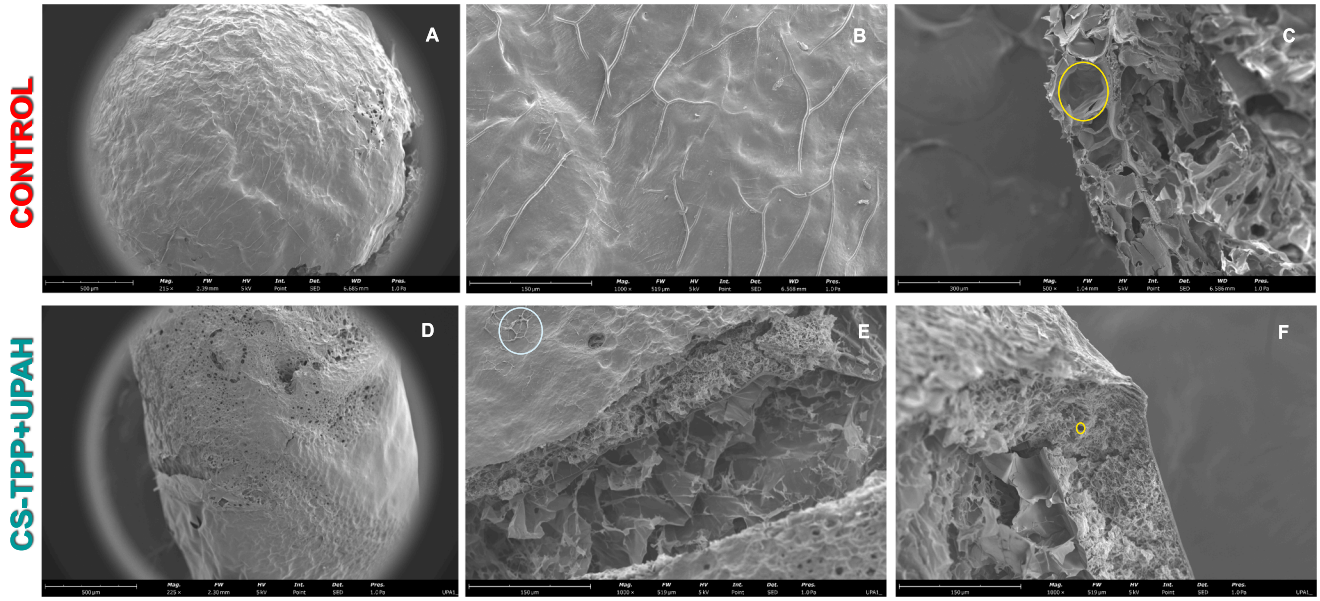

Fig. 5. SEM analysis of control and chitosan-TPP + UPAH capsules on their surface (**A**, **B**, **D**, and **E**) and the shell (**C**, **E**, and **F**) with different magnitudes: 215x (**A**); 225x (**D**); 500x (**C**); 1000x (**B**, **E**, and **F**).

control to the UPAH-loaded capsules, there is a smoother surface with less porosity on the control but a denser inside in the peptide-loaded sample (yellow circles in Fig. 5C and 5F). This corroborates the previously mentioned section 3.4, namely that incorporating peptides reduces the capsules' mesh size, resulting in a more compact capsule.

Adding peptides filled the inside, decreasing the empty spaces. However, the negative charges of these peptides can compete with TPP for the positive chitosan-charged sites, decreasing the capsule integrity. Fig. 5B and 5E highlight the presence of threadlike wrinkles on the surface of both capsule types, also previously reported by Morais da Silva et al. (2020) and Moeini et al. (2018). Since we only encapsulated about 39.3 % of peptides, the morphological differences between the control and peptide-loaded samples were not as notorious as expected.

3.6. Capsule IR spectra

Fig. 6 presents the normalized FTIR transmittance spectra of chitosan-TPP capsules with (sample) and without any peptides (control).

Chitosan-TPP + UPAH has a similar FTIR spectrum to the control, with eight major vibration modes: 3194 cm^{-1}, 2882 cm^{-1}, 1634 cm^{-1}, 1532 cm^{-1}, 1378/1216 cm^{-1}, 1152 cm^{-1}, 890 cm^{-1} and 700–600 cm^{-1} range. The stretching vibration of the hydroxyl, amino, and amide groups in chitosan typically appears between 3300 and 3450 cm^{-1} (Du et al., 2019); however, this peak shifted to 3194 cm^{-1} in all analyzed samples. Amide B, characteristic of the C-H stretch, peaked at 2882 cm^{-1} (Chatterjee et al., 2022). Amide I, a characteristic peak of C = O stretching vibrations, typically found between 1600 and 1700 cm^{-1} (Carvalho et al., 2018), appeared at 1634 cm^{-1} in chitosan-TPP + UPAH capsules, and amide II (–NH_2 bending vibrations of chitosan) at 1532 cm^{-1} (Coscueta, Sousa, Reis, & Pintado, 2021). The peak at 1378 and 1216 cm^{-1} resulted from the symmetrical deformation of CH_3 and the vibrations of the C-O of the chitosan molecule (Zeng et al., 2021). Thus, the peak between 1216 and 1152 cm^{-1} might derive from P = O stretching in TPP molecules, whereas the 890 cm^{-1} peak likely corresponded to antisymmetric stretching of the P–O bond with P–O–P (Zhao et al., 2022). The interaction pattern of chitosan and TPP was in the 780–600 cm^{-1} range, suggesting these links have symmetric stretching modes (Du et al., 2019). We observed very few differences in loaded and non-loaded capsules, probably due to the low encapsulation efficiency.

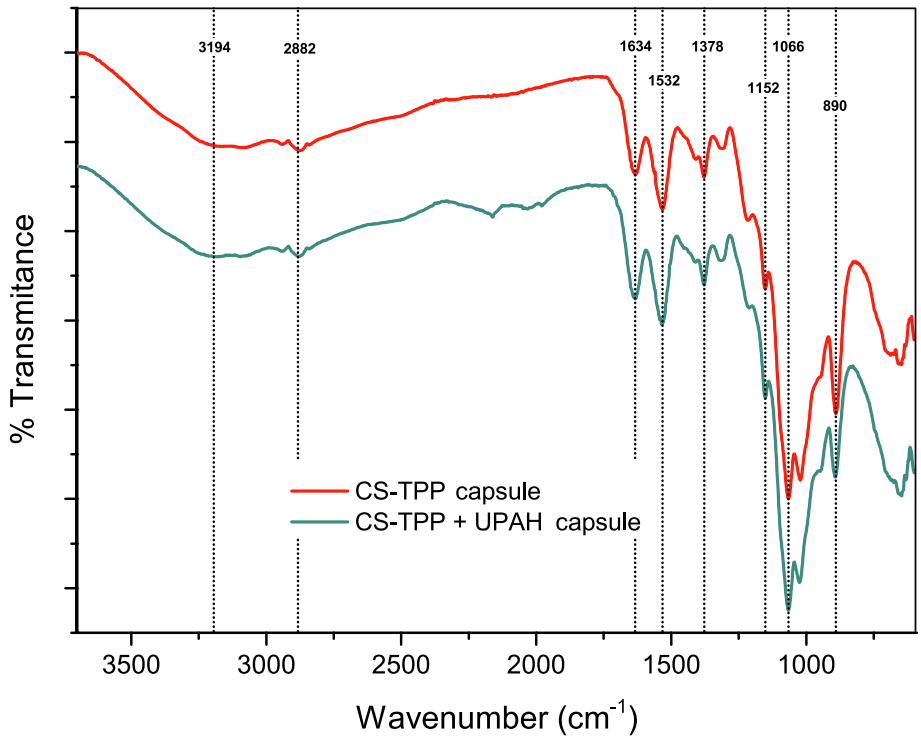

Fig. 6. FTIR spectra of control and chitosan-TPP + UPAH capsules.

3.7. Controlled peptide release

We examined the UPAH release from chitosan-TPP capsules in simulated mouth, stomach, and intestine environments using the INFOGEST protocol (Brodkorb et al., 2019). Given that digestive enzymes do not degrade chitosan, for Test A we used an enzyme-free model for this analysis (Yuan et al., 2017). Fig. 7 displays the release pattern of UPAH peptides from these capsules through the digestive tract.

The chitosan-TPP + UPAH capsules released roughly 58 % of their content, with the majority (about 51 %) occurring during the intestinal phase (120 to 240 min). This release rate can be linked to the surrounding pH and chitosan's interactions with TPP or collagen hydrolysates (Ravishankar & Dhamodharan, 2020; Yuan et al., 2017). In the acidic gastric environment, chitosan gains a positive charge, promoting ionic bonds with TPP's negative-charged groups or peptide chain charges. This means chitosan-TPP maintains a strong structure in the stomach, with peptides attaching to chitosan. However, in the higher pH of the intestine, chitosan loses its charge, increasing capsule porosity and peptide release (Ravishankar & Dhamodharan, 2020).

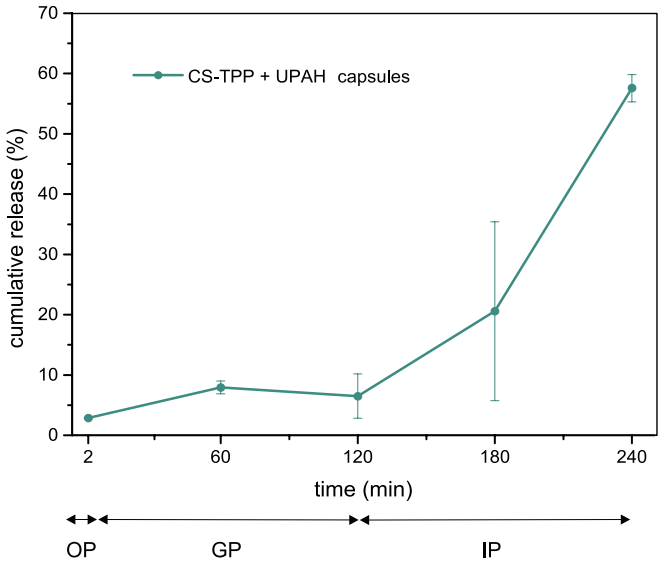

Fig. 7. Cumulative release of UPAH across the simulated gastrointestinal tract. OP: oral phase; GP: gastric phase; IP: intestinal phase.

Some peptides may remain attached to the chitosan-TPP matrix made during capsule production, keeping the cumulative release below 100 %. The peptide release also depends on the capsule's and peptide's hydrophobicity. Notably, many peptides in the samples are polar, binding efficiently to chitosan. Nevertheless, a hydrophobic segment may be released first or retained based on capsule ionic strength. Blending chitosan with compounds like polyphosphoric acid might enhance capsule swelling, prompting earlier peptide release in acidic settings (Yuan et al., 2018). In summary, chitosan-TPP encapsulation offers a promising intestinal delivery method for most collagen peptides. Still, more research is needed to understand the capsule's behavior and how biological fluids affect collagen hydrolysates (Yuan et al., 2017).

3.8. Gastrointestinal peptide digestion

We analyzed the behavior of UPAH in the gastrointestinal tract by observing size changes through HPSEC (Fig. 8). In this test (Test B), we included proteolytic enzymes to assess the hydrolysis of the hydrolysates during the oral, gastric, and intestinal phases.

Fig. 8A shows no change in the control and UPAH in the oral phase. In the gastric phase with pepsin (Fig. 8B), the sample peak slightly broadened, signifying minimal hydrolysis. However, the addition of pancreatin in the intestinal phase (Fig. 8C) significantly altered the UPAH's profile, with prominent peaks in the control due to enzyme presence.

Detailed insights on peptide size changes are available in Fig. 8D, where enzyme and product signals were subtracted. The most noticeable peptide size changes occurred in the intestinal phase (Fig. 8E). Interestingly, larger peptides (>10 kDa) emerged in the gastric and intestinal phases. This phenomenon might be because alcalase did not completely

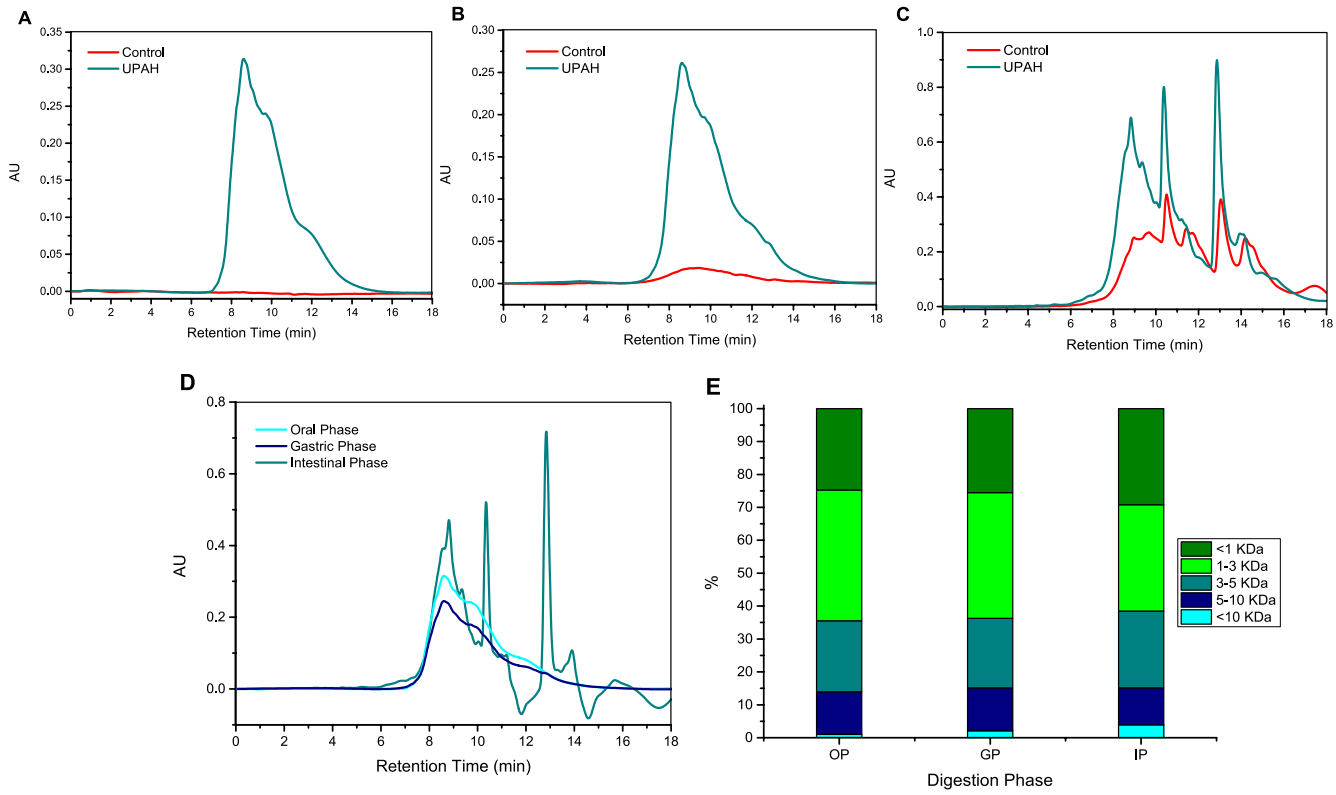

Fig. 8. HPSEC results of UPAH gastrointestinal tract simulation; **A**-HPSEC chromatograms of control and sample in Oral phase (OP); **B**-HPSEC chromatograms of control and sample in Gastric phase (GP); **C**-HPSEC chromatograms of control and sample in Intestinal phase (IP); **D**-HPSEC chromatograms of subtracted samples in the three digestion phases; **E**- peptide size distribution in all digestion phases.

break down native collagen, which remains insoluble at pH 7. During digestion, gastric and intestinal enzymes could have released these new polypeptides. Additionally, the primary detection method might miss some free amino acids, suggesting more intense hydrolysis might have occurred, especially in the < 1 kDa fraction. An in-depth amino acid analysis could clarify this.

Test B's results highlighted minor hydrolysis changes in UPAH throughout digestion, except during the intestinal phase. This observation hints that encapsulation might be unnecessary. Nevertheless, it is vital to factor in the bioactive properties; therefore, we assessed the ORAC and iACE during the three digestion phases to understand human digestion's effects on collagen peptide qualities. Fig. 9A revealed a notable rise (about tenfold) in antioxidant activity in the UPAH. Digestion might cause hydrolysis, boosting antioxidant activity (Felician et al., 2018). Conversely, iACE activity dropped from 35 % to 5 % in UPAH during digestion, as seen in Fig. 9B. Past studies have highlighted the pronounced impacts of orally delivered collagen peptides upon gastrointestinal digestion, mainly due to extensive enzyme breakdown (Felician et al., 2018).

Fine-tuning the process for specific conditions or diseases remains

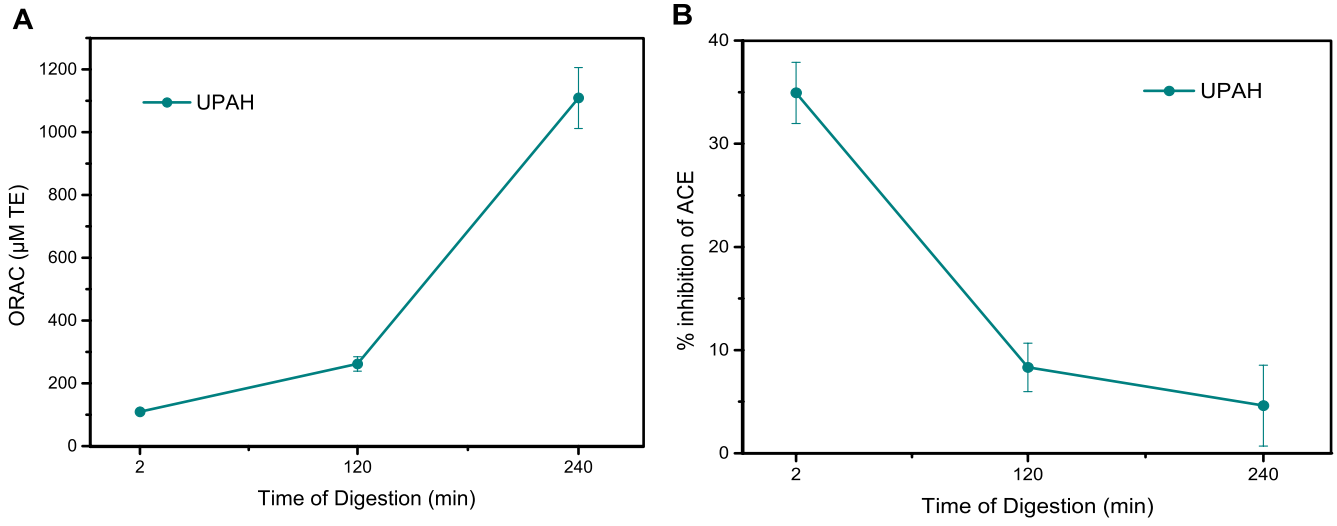

Fig. 9. Bioactivity variation across the simulated gastrointestinal tract.; **A**-Potential antioxidant activity (ORAC; μM TE); **B**-Potential antihypertensive activity (iACE; % of inhibited ACE).

crucial. For instance, encapsulation might help preserve iACE activity but not antioxidant activity. Hence, choosing a strategy based on the targeted condition is more effective.

3.9. Biocompatibility

We assessed the biocompatibility and non-toxicity of collagen hydrolysates on Caco-2 cells using samples from the final intestinal phase, which measured 451 ± 146 μg collagen hydrolysate mL^{-1}. Fig. 10 displays the metabolic inhibition percentages. The data confirms that metabolic inhibition remains below the accepted threshold of 30 % (Coscueta, Brassesco, & Pintado, 2021a; Coscueta, Sousa, Reis, & Pintado, 2021), indicating no toxicity in Caco-2 cells when exposed to digested UPAH, aligning with some existing literature findings (Pateiro et al., 2020). It is worth noting that these values approach the threshold; hence, increasing the protein concentration beyond roughly 3600 ug mL^{-1} might risk cytotoxicity. Further testing is essential for confirming this alternative's safety. While Caco-2 cells serve as a standard to study absorption mechanisms in intestinal epithelial cells, their origin in the colon means they consist only of absorptive cells. As a result, they differ from typical intestinal epithelium cells, which include a mix of cell types. Moreover, Caco-2 cells, being cancer-derived, exhibit gene expression distinct from regular human gut epithelial cells (Pateiro et al., 2020).

4. Conclusions

In this study, we have investigated the potential of Atlantic codfish skin-derived collagen hydrolysates for nutraceutical applications, employing a deep eutectic solvent for extraction and alcalase for enzymatic hydrolysis. Our findings highlight the effectiveness of this approach in producing bioactive marine collagen hydrolysates. Using chitosan-TPP capsules as delivery vehicles to ensure a controlled release in the intestine revealed a lower-than-anticipated encapsulation rate (39 %). This outcome underscores the need for further research into optimizing encapsulation conditions, considering factors like peptide diversity, ionic strength, pH, and capsule composition. Importantly, our cytotoxicity assessments using Caco-2 cells confirmed the biocompatibility of these hydrolysates, reinforcing their potential for health-related applications. While integrating eutectic solvents with enzymatic hydrolysis demonstrates promise, particularly in enhancing yields from codfish skins, our study suggests that encapsulation need and efficacy depend highly on the targeted bioactivity and intended therapeutic application. Therefore, future studies should focus on refining the extraction and hydrolysis processes and tailoring encapsulation strategies to specific health conditions or diseases. This approach will be crucial in fully realizing the potential of marine resources in blue biorefinery contexts and advancing the field of nutraceutical development.

Funding

This work was supported by National Funds from FCT - Fundação para a Ciência e a Tecnologia through project UIDB/50016/2020. Also, this work was developed within the scope of the project CICECO-Aveiro Institute of Materials, UIDB/50011/2020, UIDP/50011/2020 & LA/P/0006/2020, financed by national funds through the FCT/MCTES (PIDDAC).

Declaration of competing interest

The authors declare that they have no known competing financial interests or personal relationships that could have appeared to influence the work reported in this paper.

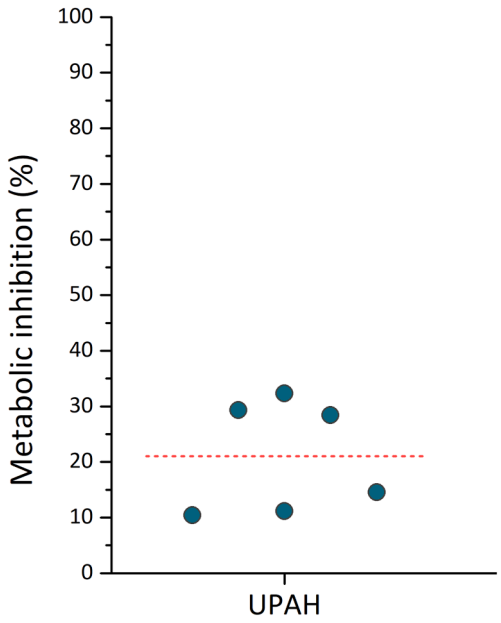

Fig. 10. Cytotoxicity results expressed as the percentage of metabolic inhibition in Caco-2 cells.

Data availability

Data will be made available on request.

Acknowledgments

The author B.M.C Vaz thanks FCT for the doctoral grant (2022.13816.BD).

References

Agyei, D., Ongkudon, C. M., Wei, C. Y., Chan, A. S., & Danquah, M. K. (2016). Bioprocess challenges to the isolation and purification of bioactive peptides. *Food and Bioproducts Processing, 98*, 244–256. https://doi.org/10.1016/J.FBP.2016.02.003

Ahn, C. B., Jeon, Y. J., Kim, Y. T., & Je, J. Y. (2012). Angiotensin i converting enzyme (ACE) inhibitory peptides from salmon byproduct protein hydrolysate by Alcalase hydrolysis. *Process Biochemistry, 47*(12), 2240–2245. https://doi.org/10.1016/j.procbio.2012.08.019

Alves, A. L., Reis, R. L., Marques, A. L. P., Martins, E., & Silva, T. H. (2017). Cosmetic Potential of Marine Fish Skin Collagen. *Cosmetics, 4*(39), 1–16. https://doi.org/10.3390/cosmetics4040039

Bai, C., Wei, Q., & Ren, X. (2017). Selective Extraction of Collagen Peptides with High Purity from Cod Skins by Deep Eutectic Solvents. *American Chemical Society: Sustainable Chemistry & Engineering, 5*, 7220–7227. https://doi.org/10.1021/acssuschemeng.7b01439

M.P. Batista N. Fernández F.B. Gaspar M. Bronze do R., & Duarte, A. R. C. Extraction of Biocompatible Collagen From Blue Shark Skins Through the Conventional Extraction Process Intensification Using Natural Deep Eutectic Solvents Frontiers in Chemistry 10 2022 10.3389/fchem.2022.937036.

M. Bisht M. MartinS A.C.R. Dias v., Ventura, S. P. M., & Coutinho, J. A. P. Uncovering the potential of aqueous solutions of deep eutectic solvents on the extraction and purification of collagen type I from Atlantic codfish (Gadus morhua) The Royal Society of Chemistry 00 2021 1 9 10.1039/d1gc01432c.

Brodkorb, A., Egger, L., Alminger, M., Alvito, P., Assunção, R., Ballance, S., … Recio, I. (2019). INFOGEST static in vitro simulation of gastrointestinal food digestion. *Nature Protocols, 14*(4), 991–1014. https://doi.org/10.1038/s41596-018-0119-1

Carvalho, A. M., Marques, A. P., Silva, T. H., & Reis, R. L. (2018). Evaluation of the Potential of Collagen from Codfish Skin as a Biomaterial for Biomedical Applications. *Marine Drugs, 16*(495), 1–14. https://doi.org/10.3390/md16120495

Chatterjee, N. S., Sukumaran, H. G., Dara, P. K., Ganesan, B., Ashraf, M., Anandan, R., Mathew, S., & Nagarajarao, R. C. (2022). Nano-encapsulation of curcumin in fish collagen grafted succinyl chitosan hydrogel accelerates wound healing process in experimental rats. *Food Hydrocolloids for Health, 2*(100061), 1–10. https://doi.org/10.1016/j.fhfh.2022.100061

Chi, C. F., Cao, Z. H., Wang, B., Hu, F. Y., Li, Z. R., & Zhang, B. (2014). Antioxidant and functional properties of collagen hydrolysates from Spanish mackerel skin as influenced by average molecular weight. *Molecules, 19*(8), 11211–11230. https://doi.org/10.3390/molecules190811211

Cho, W., Park, J., Lee, M., Park, S. H., Jung, J., Kim, J., Eun, S., & Kim, J. (2023). Gly-Pro-Val-Gly-Pro-Ser Peptide Fish Collagen Improves Skin Moisture and Wrinkles with Ameliorated the Oxidative Stress and Pro-inflammatory Factors in Skin Photoaging Mimic Models. *Preventive Nutrition and Food Science, 28*(1), 50–60. https://doi.org/10.3746/pnf.2023.28.1.50

D. Coppola M. Oliviero G.A. Vitale C. Lauritano I.D. Ambra S. Iannace D. de Pascale Marine Collagen from Alternative and Sustainable Sources : Extraction Processing and Applications. Marine Drugs 18 214 2020 1 23 https://doi.org/doi:10.3390/md18040214.

Coscueta, E. R., Brassesco, M. E., & Pintado, M. (2021a). Collagen-based bioactive bromelain hydrolysate from salt-cured cod skin. *Applied Sciences (Switzerland), 11*(18). https://doi.org/10.3390/app11188538

E.R. Coscueta M.E. Brassesco M. Pintado Salt-cured Atlantic cod skin: A sustainable source of acid-soluble type I collagen 2021 https://doi.org/10.20944/preprints202102.0378.v1.

Coscueta, E. R., Campos, D. A., Osório, H., Nerli, B. B., & Pintado, M. (2019). Enzymatic soy protein hydrolysis: A tool for biofunctional food ingredient production. *Food Chemistry: X, 1*. https://doi.org/10.1016/j.fochx.2019.100006

Coscueta, E. R., Reis, C. A., & Pintado, M. (2020). Phenylethyl isothiocyanate extracted from watercress by-products with aqueous micellar systems: Development and optimisation. *Antioxidants, 9*(8), 1–11. https://doi.org/10.3390/antiox9080698

Coscueta, E. R., Sousa, A. S., Reis, C. A., & Pintado, M. (2021). Chitosan-olive oil microparticles for phenylethyl isothiocyanate delivery: Optimal formulation. *PLoS ONE, 16*(5). https://doi.org/10.1371/journal.pone.0248257.

Du, Z., Liu, J., Zhang, T., Yu, Y., Zhang, Y., Zhai, J., Huang, H., Wei, S., Ding, L., & Liu, B. (2019). A study on the preparation of chitosan-tripolyphosphate nanoparticles and its entrapment mechanism for egg white derived peptides. *Food Chemistry, 286*, 530–536. https://doi.org/10.1016/j.foodchem.2019.02.012

Espinales, C., Romero-Peña, M., Calderón, G., Vergara, K., Cáceres, P. J., & Castillo, P. (2023). Collagen, protein hydrolysates and chitin from by-products of fish and shellfish: An overview. In *Heliyon* (Vol. 9, Issue 4)Elsevier Ltd.. https://doi.org/10.1016/j.heliyon.2023.e14937

Felician, F. F., Xia, C., Qi, W., & Xu, H. (2018). Collagen from Marine Biological Sources and Medical Applications. *Chemistry and Biodiversity, 15*(5). https://doi.org/10.1002/cbdv.201700557

Fernandez Cunha, M., Coscueta, E. R., Brassesco, M. E., Marques, R., Neto, J., Almada, F., Gonçalves, D., & Pintado, M. (2023). Exploring Bioactivities and Peptide Content of Body Mucus from the Lusitanian Toadfish Halobatrachus didactylus. *Molecules, 28*(18), 6458. https://doi.org/10.3390/molecules28186458

Gharibzahedi, S. M. T., Smith, B., & Altintas, Z. (2022). Bioactive and health-promoting properties of enzymatic hydrolysates of legume proteins: A review. *Critical Reviews in Food Science and Nutrition*. https://doi.org/10.1080/10408398.2022.2124399

Hanachi, A., Bianchi, A., Kahn, C. J. F., Velot, E., Arab-Tehrany, E., Cakir-Kiefer, C., & Linder, M. (2022). Encapsulation of Salmon Peptides in Marine Liposomes: Physico-Chemical Properties, Antiradical Activities and Biocompatibility Assays. *Marine Drugs, 20*(4). https://doi.org/10.3390/md20040249

Himaya, S. W. A., Ngo, D. H., Ryu, B., & Kim, S. K. (2012). An active peptide purified from gastrointestinal enzyme hydrolysate of Pacific cod skin gelatin attenuates angiotensin-1 converting enzyme (ACE) activity and cellular oxidative stress. *Food Chemistry, 132*(4), 1872–1882. https://doi.org/10.1016/j.foodchem.2011.12.020

Hsu, K.-C. (2010). Purification of antioxidative peptides prepared from enzymatic hydrolysates of tuna dark muscle by-product. *Food Chemistry, 122*(1), 42–48.

Ishak, N. H., & Sarbon, N. M. (2018). A Review of Protein Hydrolysates and Bioactive Peptides Deriving from Wastes Generated by Fish Processing. *Food and Bioprocess Technology, 11*(1), 2–16. https://doi.org/10.1007/s11947-017-1940-1

Ito, N., Seki, S., & Ueda, F. (2018). Effects of composite supplement containing collagen peptide and ornithine on skin conditions and plasma IGF-1 levels—A randomized, double-blind, placebo-controlled trial. *Marine Drugs, 16*(12). https://doi.org/10.3390/md16120482

Jafari, H., Lista, A., Siekapen, M. M., & Gha, P. (2020). Fish Collagen: Extraction, Characterization, and Applications for Biomaterials Engineering. *Polymers, 12*(2230), 1–37. https://doi.org/10.3390/polym12102230

Jafarpour, A., Gomes, R. M., Gregersen, S., Sloth, J. J., Jacobsen, C., & Moltke Sørensen, A. D. (2020). Characterization of cod (Gadus morhua) frame composition and its valorization by enzymatic hydrolysis. *Journal of Food Composition and Analysis, 89*, 1–12. https://doi.org/10.1016/j.jfca.2020.103469

F. Khawli al, Pateiro, M., Domínguez, R., Lorenzo, J. M., Gullón, P., Kousoulaki, K., Ferrer, E., Berrada, H., & Barba, F. J. Innovative green technologies of intensification for valorization of seafood and their by-products Marine Drugs 17 12 2019 1 20 10.3390/md17120689.

Lajmi, K., Gómez-Estaca, J., Hammami, M., & Martínez-Alvarez, O. (2019). Upgrading collagenous smooth hound by-products: Effect of hydrolysis conditions, in vitro gastrointestinal digestion and encapsulation on bioactive properties. *Food Bioscience, 28*, 99–108. https://doi.org/10.1016/j.fbio.2019.01.014

Liu, H., Wang, C., Li, C., Qin, Y., Wang, Z., Yang, F., Li, Z., & Wang, J. (2018). A functional chitosan-based hydrogel as a wound dressing and drug delivery system in the treatment of wound healing. *Royal Society of Chemistry, 8*, 7533–7549. https://doi.org/10.1039/c7ra13510f

López-Morales, C. A., Vázquez-Leyva, S., Vallejo-Castillo, L., Carballo-Uicab, G., Muñoz-García, L., Herbert-Pucheta, J. E., Zepeda-Vallejo, L. G., Velasco-Velázquez, M., Pavón, L., Pérez-Tapia, S. M., & Medina-Rivero, E. (2019). Determination of Peptide Profile Consistency and Safety of Collagen Hydrolysates as Quality Attributes. *Journal of Food Science, 84*(3), 430–439. https://doi.org/10.1111/1750-3841.14466

Mildenberger, J., Remm, M., & Atanassova, M. (2021). Self-assembly potential of bioactive peptides from Norwegian sea cucumber Parastichopus tremulus for development of functional hydrogels. *LWT, 148*. https://doi.org/10.1016/j.lwt.2021.111678

Moeini, A., Cimmino, A., Dal Poggetto, G., Di Biase, M., Evidente, A., Masi, M., Lavermicocca, P., Valerio, F., Leone, A., Santagata, G., & Malinconico, M. (2018). Effect of pH and TPP concentration on chemico-physical properties, release kinetics and antifungal activity of Chitosan-TPP-Ungeremine microbeads. *Carbohydrate Polymers, 195*, 631–641. https://doi.org/10.1016/j.carbpol.2018.05.005

P.M. Morais da Silva N.G. Camparotto T. de Figueiredo Neves K.T. Grego Lira V.R. Mastelaro S.F. Picone C., & Prediger, P. Effective removal of basic dye onto sustainable chitosan beads: Batch and fixed-bed column adsorption, beads stability and mechanism Sustainable Chemistry and Pharmacy 18 2020 10.1016/j.scp.2020.100348.

Nasri, R., Hamdi, M., Touir, S., Li, S., Karra-Chaâbouni, M., & Nasri, M. (2021). Development of delivery system based on marine chitosan: Encapsulationand release kinetic study of antioxidant peptides from chitosan microparticle. *International Journal of Biological Macromolecules, 167*, 1445–1451. https://doi.org/10.1016/j.ijbiomac.2020.11.098

Neves, A. C., Harnedy, P. A., O'Keeffe, M. B., Alashi, M. A., Aluko, R. E., & FitzGerald, R. J. (2017). Peptide identification in a salmon gelatin hydrolysate with antihypertensive, dipeptidyl peptidase IV inhibitory and antioxidant activities. *Food Research International, 100*, 112–120. https://doi.org/10.1016/j.foodres.2017.06.065

Oliveira, V. de M., Assis, C. R. D., Costa, B. de A. M., Neri, R. C. de A., Monte, F. T., Freitas, H. M. S. da C. V., França, R. C. P., Santos, J., Bezerra, R. de S., & Porto, A. L. F. (2021). Physical, biochemical, densitometric and spectroscopic techniques for characterization collagen from alternative sources: A review based on the sustainable valorization of aquatic by-products. *Journal of Molecular Structure, 1224*. https://doi.org/10.1016/j.molstruc.2020.129023.

Pateiro, M., Munekata, P. E. S., Tsatsanis, C., Domínguez, R., Zhang, W., Barba, F. J., & Lorenzo, J. M. (2020). *Evaluation of the protein and bioactive compound bioaccessibility/bioavailability and cytotoxicity of the extracts obtained from aquaculture and fisheries by-products* (Vol. 92,, 97–125. https://doi.org/10.1016/bs.afnr.2019.12.002

Prabha, S. P., Nagappan, S., Rathna, R., Viveka, R., & Nakkeeran, E. (2020). Blue biotechnology: A vision for future marine biorefineries. In *Refining Biomass Residues for Sustainable Energy and Bioproducts: Technology, Advances* (pp. 463–480). Elsevier Inc.. https://doi.org/10.1016/B978-0-12-818996-2.00021-1

Ravishankar, K., & Dhamodharan, R. (2020). Advances in chitosan-based hydrogels: Evolution from covalently crosslinked systems to ionotropically crosslinked superabsorbents. *Reactive and Functional Polymers, 149*(104517), 1–15. https://doi.org/10.1016/j.reactfunctpolym.2020.104517

Rodrigues, D. P., Calado, R., Ameixa, O. M. C. C., Valcarcel, J., & Vázquez, J. A. (2021). Valorisation of Atlantic codfish (Gadus morhua) frames from the cure-salting industry as fish protein hydrolysates with in vitro bioactive properties. *Lwt, 149*, 1–8. https://doi.org/10.1016/j.lwt.2021.111840

Rodrigues, C. V., Sousa, R. O., Carvalho, A. C., Alves, A. L., Marques, C. F., Cerqueira, M. T., Reis, R. L., & Silva, T. H. (2023). Potential of Atlantic Codfish (Gadus morhua) Skin Collagen for Skincare Biomaterials. *Molecules, 28*(8). https://doi.org/10.3390/molecules28083394

Schägger, H., & von Jagow, G. (1987). Tricine-Sodium Dodecyl Sulfate-Polyacrylamide Gel Electrophoresis for the Separation of Proteins in the Range from 1 to 100 kDa. *Analytical Biochemistry, 166*, 368–379.

Sun, S., Gao, Y., Chen, J., & Liu, R. (2022). Identification and release kinetics of peptides from tilapia skin collagen during alcalase hydrolysis. *Food Chemistry, 378*. https://doi.org/10.1016/j.foodchem.2022.132089

Vázquez, J. A., Meduíña, A., Durán, A. I., Nogueira, M., Fernández-Compás, A., Pérez-Martín, R. I., & Rodríguez-Amado, I. (2019). Production of valuable compounds and bioactive metabolites from by-products of fish discards using chemical processing, enzymatic hydrolysis, and bacterial fermentation. *Marine Drugs, 17*(3). https://doi.org/10.3390/md17030139

Wauquier, F., Boutin-Wittrant, L., Bouvret, E., Le Faouder, J., Roux, V., Macian, N., Pickering, G., & Wittrant, Y. (2022). Benefits of Circulating Human Metabolites from Fish Cartilage Hydrolysate on Primary Human Dermal Fibroblasts, an Ex Vivo Clinical Investigation for Skin Health Applications. *Nutrients, 14*(23). https://doi.org/10.3390/nu14235027

Wei, B., Zhu, W., Li, K., Liu, Q., Zhang, J., Kou, H., Xu, C., He, L., & Wang, H. (2022). Natural collagen peptides-encapsulated gold nanoclusters for the simultaneous detection of multiple antibiotics in milk and molecular logic operations. *LWT, 153*. https://doi.org/10.1016/j.lwt.2021.112416

Wu, R. B., Wu, C. L., Liu, D., Yang, X. H., Huang, J. F., Zhang, J., Liao, B., & He, H. L. (2018). Antioxidant and anti-freezing peptides from salmon collagen hydrolysate prepared by bacterial extracellular protease. *Food Chemistry, 248*, 346–352. https://doi.org/10.1016/j.foodchem.2017.12.035

Yu, D., Cui, S., Chen, L., Zheng, S., Zhao, D., Yin, X., Yang, F., & Chen, J. (2023). Marine-Derived Bioactive Peptides Self-Assembled Multifunctional Materials. *Antioxidant and Wound Healing. Antioxidants, 12*(6). https://doi.org/10.3390/antiox12061190

Yuan, D., Jacquier, J. C., & O'Riordan, E. D. (2017). Entrapment of protein in chitosan-tripolyphosphate beads and its release in an in vitro digestive model. *Food Chemistry, 229*, 495–501. https://doi.org/10.1016/j.foodchem.2017.02.107

Yuan, D., Jacquier, J. C., & O'Riordan, E. D. (2018). Entrapment of proteins and peptides in chitosan-polyphosphoric acid hydrogel beads: A new approach to achieve both high entrapment efficiency and controlled in vitro release. *Food Chemistry, 239*, 1200–1209. https://doi.org/10.1016/j.foodchem.2017.07.021

Zeng, W., Hui, H., Liu, Z., Chang, Z., Wang, M., He, B., & Hao, D. (2021). TPP ionically cross-linked chitosan/PLGA microspheres for the delivery of NGF for peripheral

nerve system repair. *Carbohydrate Polymers, 258*. https://doi.org/10.1016/j.carbpol.2021.117684

Zhang, Y., Zhou, F., Zhao, M., Ning, Z., Sun-Waterhouse, D., & Sun, B. (2017). Soy peptide aggregates formed during hydrolysis reduced protein extraction without decreasing their nutritional value. *Food & Function, 8*(12), 4384–4395. https://doi.org/10.1039/C7FO00812K

Zhao, M., He, H., Guo, D., Zhang, X., Jia, L., Hou, T., & Ma, A. (2022). Chitosan oligosaccharides-tripolyphosphate microcapsules as efficient vehicles for desalted duck egg white peptides-calcium: Fabrication, entrapment mechanism and in vivo calcium absorption studies. *LWT, 154*. https://doi.org/10.1016/j.lwt.2021.112869